On the Design of An Equivalent Circuit Model for Lithium-Ion Batteries Operating Across Broad Current Ranges

Nikhil Biju *,** Huazhen Fang *

* Department of Mechanical Engineering, University of Kansas, USA ** Gamma Technologies, USA

Abstract: Equivalent circuit models have gained significant use in lithium-ion battery management systems, because of their computational efficiency and convenience for use. However, none of the existing ones by design is suitable for charging/discharging across low to high C-rates. In this paper, we propose a new equivalent circuit model, called BattX, to address the challenge. The BattX model develops and combines circuit analogs to not only simulate the main dynamic processes in the electrode and electrolyte phases and in the temperature evolution, but also capture their effects on the terminal voltage. The design presents a correspondence with electrochemical modeling to comprehensively grasp a battery's dynamic behavior, thus ensuring a predictive capability over broad C-rate ranges. We further present a multi-pronged parameter identification approach to extract the model's parameters from measurement data. Extensive simulations involving different scenarios and load profiles are conducted to show the model's high predictive accuracy when the current ranges are wide.

Keywords: Lithium-ion batteries; battery management systems; dynamic modeling; equivalent circuit models

1. INTRODUCTION

A breakthrough in electrochemical energy storage, lithiumion batteries (LiBs) has penetrated into various key sectors to drive electrification and decarbonization. They stand on some significant merits such as high energy and power density and long life but still rely on battery management systems to provide desired levels of performance, safety, and longevity. Many battery management tasks increasingly require the use of dynamic models, among which equivalent circuit models (ECMs) have proven useful and promising.

ECMs are circuit analogs composed of electrical components to simulate a cell's dynamic behavior, capture different phenomena in charging/discharging, and track state-of-charge (SoC) and power capability. With simple structures, they are easy to calibrate and scalable to large LiB systems comprising many cells. Further, they are governed by a set of several first-order ordinary differential equations and thus amenable to computation and implementation. Due to these benefits, they have emerged as the most popular models especially for real-world battery management systems with limited computing resources. The literature has presented an array of ECMs. A basic one, called the Rint model, cascades an open-circuit voltage (OCV) source with an internal resistor, in which the voltage source is SoC-dependent (He et al., 2011). One can add to the Rint model a set of serially connected RC pairs to describe the transient behavior in a cell's voltage response, leading to the socalled Thevenin's model (Mousavi G. and Nikdel, 2014; Plett, 2015). Depending on the number of RC pairs used, the model can be set to capture transients at multiple time scales (Tian et al., 2020b). Different ways have been studied to modify the Thevenin's model for better accuracy. For example, the study

in (Plett, 2015; Wang et al., 2017) incorporates hysteresis in charging/discharging; in (Lee et al., 2018; Chen and Rincon-Mora, 2006; Hu et al., 2012; Weng et al., 2014), different circuit parameters (e.g., the internal resistance) are made dependent on the SoC, temperature, or current loads, and the OCV is parameterized using different function forms for higher fitting accuracy. Recently, a growing number of investigations have explored to develop ECMs drawing upon electrochemical modeling, even though these two modeling approaches used to be disparate. The work in (Tian et al., 2018, 2020a) proposes the nonlinear double capacitor model to approximate the ion diffusion in the electrodes of a cell and characterizes the nonlinear voltage behavior simultaneously. This model is interpretable as a reduced-order version of the single particle model, and it is further supplemented in (Movahedi et al., 2022) with a data-based voltage hysteresis model to attain better accuracy. The study in (Li et al., 2021) derives an ECM using circuit elements to describe charge transfer and diffusion potentials; the derivation also helps explain some conventional ECMs from an electrochemical perspective.

The structural simplicity of ECMs facilitates fast computation, but also imposes restrictions on the prediction accuracy. Most of today's ECMs are accurate enough for only low to medium currents, around or below 1C. Although this level of accuracy is acceptable for many applications, it falls short from meeting the needs of some emerging battery-powered systems. One example is electric Vertical Takeoff and Landing (eVTOL) vehicles, which involves high C-rate discharging in the takeoff and landing phases and necessitates precise models to fulfill high-stakes safety requirements (Bills et al., 2020). This poses an interesting and important question: *Is it possible to develop an ECM that can present accurate prediction over broad C-rate ranges, and how?*

^{*} Contact: N. Biju (biju@gtisoft.com); H. Fang (fang@ku.edu).

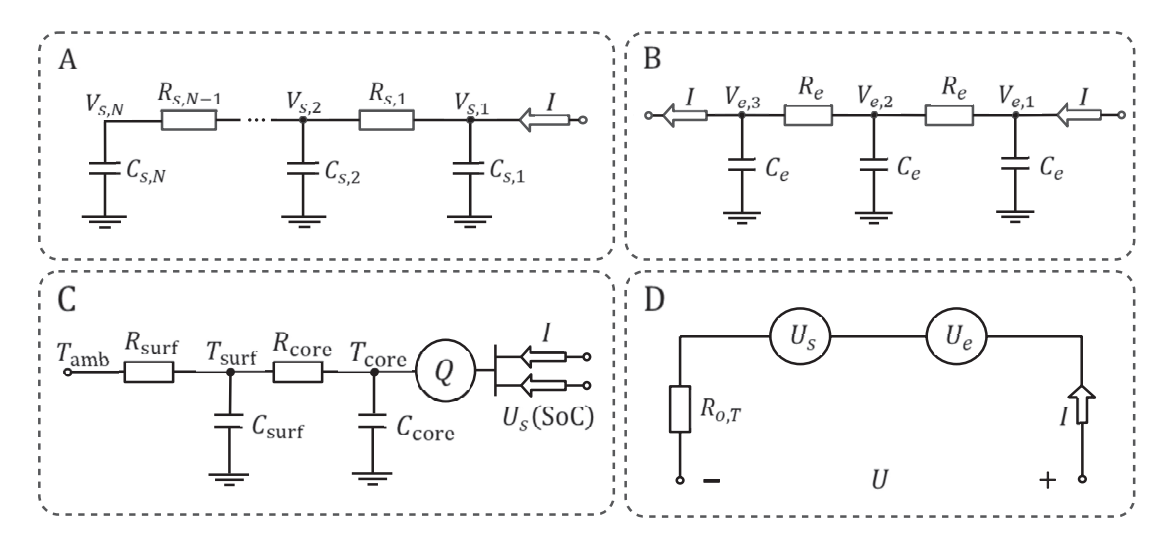


Fig. 1. The BattX model comprising: sub-circuit A to simulate the lithium-ion diffusion in the electrode phase; sub-circuit B to simulate the lithium-ion diffusion in the electrolyte phase; sub-circuit C to simulate heat conduction and convection; and sub-circuit D to simulate the terminal voltage.

To answer the question, we turn attention to electrochemical modeling. This model approach explicitly describes electrochemical reactions, transport of lithium ions, and distribution of charge and potential inside a LiB cell. Compared to ECMs, electrochemical models, e.g., the Doyle-Fuller-Newman model (Doyle et al., 1993), generally present finergrained description and thus higher accuracy over wide current rages, while being more expensive computationally. Taking inspirations from electrochemical modeling, we propose to use coupled circuits to simulate a LiB cell's electrode, electrolyte, and thermal dynamics as well as their effects on the terminal voltage. This then leads to a new ECM for LiBs, called BattX, which, for the first time, expands the reach of ECMs to prediction over low to high currents. The BattX model also retains compact and physically interpretable structures to offer high computational efficiency and invoke conduciveness to understanding. Based on the above, this paper delivers three contributions. First, we show the principled design of the BattX model and explain the rationale underlying the design. Second, we develop a multi-pronged parameter identification approach to extract the parameters of the BattX model from measurement data made on LiBs. Finally, to validate the BattX model, we perform extensive simulations to evaluate its effectiveness and accuracy, using a pseudo-two-dimensional electrochemical model as a benchmark reference.

The rest of the paper is organized as follows. Section 2 presents the BattX model design and the essential reasoning behind it. Section 3 develops the parameter identification pipeline of the model. Section 4 evaluates the model using experimental data. Finally, Section 5 offers concluding remarks.

2. THE BATTX MODEL

In this section, we show the circuit structure and governing equations of the BattX model and delineate the main idea of the circuit design. For the detailed modeling rationale, the reader is referred to (Biju and Fang, 2023).

At the core, the BattX model attempts to characterize the multiple major dynamic processes innate to a LiB cell in order to capture the cell's behavior from low to high current rates. This is akin to electrochemical modeling to a certain extent, but a main difference is that the BattX model leverages circuit analogs to simulate the processes. Fig. 1 shows the overarching structure of the model. As is seen, it consists of four coupled sub-circuits, which are labeled as A to D. These sub-circuits are designed to approximate the cell's electrodephase diffusion, electrolyte-phase diffusion, thermal evolution, and voltage response, respectively.

To begin with, sub-circuit A uses a chain of resistors and capacitors to approximate the lithium-ion diffusion in the electrode phase. Its governing equations are

chase. Its governing equations are
$$\dot{V}_{s,1}(t) = \frac{V_{s,2}(t) - V_{s,1}(t)}{C_{s,1}R_{s,1}} + \frac{I(t)}{C_{s,1}}, \qquad (1a)$$

$$\dot{V}_{s,i}(t) = \frac{V_{s,i-1}(t) - V_{s,i}(t)}{C_{s,i}R_{s,i-1}} + \frac{V_{s,i+1}(t) - V_{s,i}(t)}{C_{s,i}R_{s,i}}, \qquad (1b)$$

$$\dot{V}_{s,N}(t) = \frac{V_{s,N-1}(t) - V_{s,N}(t)}{C_{s,N}R_{s,N-1}}, \qquad (1c)$$

$$\dot{V}_{s,i}(t) = \frac{V_{s,i-1}(t) - V_{s,i}(t)}{C_{s,i}R_{s,i-1}} + \frac{V_{s,i+1}(t) - V_{s,i}(t)}{C_{s,i}R_{s,i}}, \quad (1b)$$

$$\dot{V}_{s,N}(t) = \frac{V_{s,N-1}(t) - V_{s,N}(t)}{C_{s,N}R_{s,N-1}},$$
(1c)

where i = 2, ..., N - 1. Here, I is the applied current, with I > 0 for charging and I < 0 for discharging, $V_{s,j}$ for j = $1, \ldots, N$ are the voltages across the individual capacitors $C_{s,j}$, $R_{s,j}$ are the resistors that the current must flow through, and the subscript s refers to the solid phase. We set $0 \leq V_{s,j} \leq 1$ for the purpose of normalization and then define the SoC as the percentage ratio of the currently available charge over the total charge capacity, which is

SoC =
$$\frac{\sum_{j=1}^{N} C_{s,j} V_{s,j}}{\sum_{j=1}^{N} C_{s,j}} \times 100\%.$$

That is, SoC = 100% when $V_{s,j}=1$ for all j, and SoC = 0 when $V_{s,j}=0$ for all j. A brief interpretation of sub-circuit A is as follows, with more details available in (Biju and Fang, 2023). Overall, the charge transfer between the capacitors in the circuit mimics the diffusion of lithium ion in the solid phase or electrode. Then, $V_{s,j}$ for $j=1,\ldots,N$ correspond to the lithium-ion concentrations at N different locations, from the surface to the center, that spread along the radius of an electrode sphere; $C_{s,j}$ for $j=1,\ldots,N$ are analogous to the volumes of the subdomains if one subdivides the electrode sphere at these

discrete locations; $R_{s,j}$ for $j=1,\ldots,N-1$ resist the charge transfer or equivalently, the solid-phase diffusion, and are hence inversely proportional to the diffusivity.

Along similar lines to sub-circuit A, sub-circuit B uses a resistor-capacitor chain to approximate the lithium-ion diffusion in the electrolyte. Its dynamics is governed by

$$\dot{V}_{e,1}(t) = \frac{V_{e,2}(t) - V_{e,1}(t)}{C_e R_e} + \frac{I(t)}{C_e},$$
 (2a)

$$\dot{V}_{e,2}(t) = \frac{V_{e,1}(t) - 2V_{e,2}(t) + V_{e,3}(t)}{C_e R_e},$$
 (2b)

$$\begin{split} \dot{V}_{e,1}(t) &= \frac{V_{e,2}(t) - V_{e,1}(t)}{C_e R_e} + \frac{I(t)}{C_e}, \\ \dot{V}_{e,2}(t) &= \frac{V_{e,1}(t) - 2V_{e,2}(t) + V_{e,3}(t)}{C_e R_e}, \\ \dot{V}_{e,3}(t) &= \frac{V_{e,2}(t) - V_{e,3}(t)}{C_e R_e} - \frac{I(t)}{C_e}, \end{split} \tag{2a}$$

where the notations in above have similar meanings as in (1), and the subscript e refers to the electrolyte. We let $V_{e,j} = 1200$ for j = 1, 2, 3 when the cell is at equilibrium. One can interpret sub-circuit B as analogous to the one-dimensional electrolytephase diffusion that is discretized along the spatial coordinate. In particular, $V_{e,j}$ for j = 1, 2, 3 can be associated with the lithium-ion concentrations at the locations of the anode, separator, and cathode, and R_e embodies resistance to the diffusion. The spatial discretization is assumed to be uniform, thus leading to the same values of R_e and C_e for each region as shown in (2).

Sub-circuit C is a lumped circuit model for the thermal dynamics, with the design inspired by (Lin et al., 2014). Here, we consider the cell to be a cylindrical one without loss of generality and concentrate its spatial dimensions into two singular points that represent the surface and core, respectively. This simplification allows to describe the evolution of the temperatures at these two points, T_{surf} and T_{core} , by

$$\dot{T}_{\text{core}}(t) = \frac{Q(t)}{C_{\text{core}}} + \frac{T_{\text{surf}}(t) - T_{\text{core}}(t)}{R_{\text{core}}C_{\text{core}}},$$
(3a)

$$\dot{T}_{\rm core}(t) = \frac{Q(t)}{C_{\rm core}} + \frac{T_{\rm surf}(t) - T_{\rm core}(t)}{R_{\rm core}C_{\rm core}}, \tag{3a}$$

$$\dot{T}_{\rm surf}(t) = \frac{T_{\rm amb}(t) - T_{\rm surf}(t)}{R_{\rm surf}C_{\rm surf}} - \frac{T_{\rm surf}(t) - T_{\rm core}(t)}{R_{\rm core}C_{\rm surf}}, \tag{3b}$$
where $T_{\rm amb}$ is the ambient temperature, $C_{\rm surf/core}$ and $R_{\rm surf/core}$

represent the thermal capacitance and resistance at the surface and core, respectively, and Q is the internal heat generation rate accompanying electrochemical reactions inside the cell during charging/discharging. From a heat transfer perspective, (3a) approximately describes the heat conduction between the cell's surface and core, and (3b) grasps the convection between the surface and the ambient environment. Further, Q is character-

$$Q = -I \left[U_s (SOC) - U_s(V_{s,1}) - R_{o,T} I \right], \tag{4}$$

where $U_s(\cdot)$ is the nonlinear OCV function, $V_{s,1}$ is defined in sub-circuit A, and $R_{o,T}$ is the internal resistance.

Finally, sub-circuit D summarizes the effects of the solidphase and electrolyte-phase dynamics on the terminal voltage. It contains two voltage sources, U_s and U_e , in series with an internal resistance $R_{o,T}$. The terminal U is given by

$$U = U_s(V_{s,1}(t)) + U_e(V_{e,1}(t), V_{e,3}(t)) + R_{o,T}I(t).$$
 (5)

Here, U_s simulates the solid-phase OCV. The open-circuit potential of solid material relies on the lithium-ion concentration at the surface of the electrode, U_s should come as a function of $V_{s,1}$, and its exact form will depend on the cell. The optimal function to capture this relationship often varies with the cell (Weng et al., 2014).

In electrochemical modeling, the electrolyte potential depends on the electrolyte concentration at the anode and cathode. We hence make U_e as a function of $V_{e,1}$ and $V_{e,3}$ and express it as

$$U_e(t) = \beta_1 \ln \left(\frac{V_{e,1}(t)}{V_{e,3}(t)} \right),$$
 (6)

where β_1 is a constant coefficient. As the last element of the model, $R_{o,T}$ is not a constant and instead depends on $V_{s,1}$ and $T_{\rm core}$. It is given by

$$R_{o,T} = R_o(V_{s,1}) \cdot \exp\left(\kappa_1 \left(\frac{1}{T_{\text{core}}} - \frac{1}{T_{\text{amb}}}\right)\right),$$
 (7)

where κ_1 is a constant coefficient. In above, the first term $R_o(V_{s,1})$ captures the dependence of $R_{o,T}$ on $V_{s,1}$ and can be approximated by a polynomial. The second term shows the temperature dependence due to the Arrhenius law. Similarly, an Arrhenius relationship can be used to capture the relationship between the electrode-phase diffusion constant and tempera-

$$R_{s,1,T} = R_{s,1} \cdot \exp\left(\kappa_2 \left(\frac{1}{T_{\text{core}}} - \frac{1}{T_{\text{amb}}}\right)\right). \tag{8}$$

Putting together all the above equations, we will obtain a complete description of the BattX model. This model is the first ECM that can predict over broad current ranges, due to the integration of the circuits approximating the electrode, electrolyte, and thermal dynamics into a whole. The model design also leads to profound comparability with electrochemical modeling. We will address the identification of the model parameters in the next section.

3. PARAMETER IDENTIFICATION FOR THE BATTX MODEL

In this section, we investigate how to determine the parameters of the BattX model. To this end, we separate the model's parameters into different groups based on the dynamic processes that they belong to or prominently influence. We then design experiments accordingly and use different current profiles to excite different dynamic processes and obtain voltage or temperature data suitable for the identification of the corresponding parameter groups. Finally, we extract the parameters from the data, group by group, through data fitting and some empirical tuning.

The identification of the SoC/OCV relationship is a standard practice and thus skipped here. We start with setting up the following parameter groups for the BattX model:

- $\Theta_{R_o}=\{\gamma_i, i=1,2,3\},$ which includes the parameters in R_o in sub-circuit D;
- $\Theta_s = \{C_{s,i}, i = 1, \dots, N, R_{s,j}, j = 1, \dots, N-1\}$, which includes the parameters of sub-circuit A;
- $\Theta_{\rm Th} = \{C_{\rm surf}, R_{\rm surf}, C_{\rm core}, R_{\rm core}\}$, which includes the parameters in the lumped thermal model in sub-circuit C;
- $\Theta_e = \{C_e, R_e, \beta_1\}$, which includes the parameters in subcircuit B and the parameters in U_e in sub-circuit D;
- $\Theta_{Arr} = \{\kappa_1, \kappa_2\}$, which includes the Arrhenius-lawrelated parameters.

By grouping the parameters as above, we can design different current input profiles to stimulate different parts of the cell's dynamics so as to identify the parameters of the corresponding groups. This multi-pronged approach includes the following steps.

Step 1: Identification of Θ_{R_o} . R_o is an integral part of the internal resistance $R_{o,T}$, and $R_o=R_{o,T}$ when $T=T_{\rm ref}$. To identify Θ_{R_o} , we apply a 0.5 C pulse current profile, which includes long enough rest periods between two consecutive pulses to allow for sufficient voltage recovery, to discharge the cell from 100% to 0% of SoC when the ambient temperature is $T_{\rm ref}$. With discharging at 0.5 C, the cell will see only a negligible increase in its temperature, and $U_e\approx 0$. For the terminal voltage U, we will see a sharp drop or jump at the beginning or end of every pulse, and this is almost solely due to the voltage change across R_o . Therefore, using the voltage jump, one can approximate R_o as

$$\tilde{R}_o(t_*) = \left| \frac{U(t_* - 1) - U(t_*)}{I} \right|,$$
(9)

where t_* is the instant after a pulse is applied. Note that we can readily determine $V_{s,1}$ with the idea that $V_{s,1} = \mathrm{SoC}$ when the cell reaches equilibrium after a long rest period and that SoC can be calculated via Coulomb counting. Collecting R_o for all t_* , we can formulate the following data fitting problem to estimate Θ_{R_o} :

$$\hat{\Theta}_{R_o} = \arg\min_{\Theta_{R_o}} \sum_{t_*} \left[\tilde{R}_o(t_*) - R_o(\Theta_{R_o}; t_*) \right]^2.$$
 (10)

Step 2: Identification of Θ_s . The number of parameters in Θ_s depends on N, and when N is large, Θ_s will be poorly identifiable to defy accurate estimation. To formulate a tractable identification problem, we assume that

$$C_{s,i} = \lambda_i C_{s,1}, \ R_{s,j} = \sigma_j R_{s,1},$$
 (11)

where λ_i and σ_i for $i=1,\ldots N$ and $j=1,\ldots N-1$ are prespecified coefficients with $\lambda_1=\sigma_1=1$, and $\sum_{i=1}^N \lambda_i C_{s,i}$ is the total capacity of the cell. This allows us to consider only two parameters, i.e., $\Theta_s=\{C_{s,1},R_{s,1}\}$, greatly facilitating the parameter estimation. Going forward, we apply a 0.5 C constant-current profile to discharge the cell from full to zero SoC. In this setting, sub-circuit A is excited, but the dynamics of sub-circuits B and C have no appreciable effects. That is, the cell's temperature remains almost the same, and $U_e\approx 0$. We can conduct data fitting as below to find out Θ_s :

$$\hat{\Theta}_{s} = \arg\min_{\Theta_{s}} \sum_{t_{k}} \left[U(t_{k}) - R_{o} \left(\hat{\Theta}_{R_{o}}; t_{k} \right) I(t_{k}) - U_{s} \left(V_{s,1} \left(\Theta_{s}; t_{k} \right); \hat{\Theta}_{U_{s}} \right) \right]^{2}, \quad (12)$$

where $\hat{\Theta}_{U_s}$ and $\hat{\Theta}_{R_o}$ have been obtained in Steps 1 and 2, and the form of $V_{s,1}(\Theta_s,t)$ is shown in (Biju and Fang, 2023).

Step 3: Identification of Θ_{Th} , Θ_{e} and Θ_{Arr} . These three groups of parameters can be identified together because both the thermal and electrolyte dynamics will substantially manifest themselves under high C-rate loads. We can fully discharge the cell at 1.5 C and a 2 C separately and then use both datasets to determine the parameters. To identify Θ_{Th} , the following data fitting problem can be considered:

$$\hat{\Theta}_{\mathrm{Th}} = \arg\min_{\Theta_{\mathrm{Th}}} \sum_{t_k} \left[T(t_k) - T_{\mathrm{surf}} \left(\hat{\Theta}_{\mathrm{Th}}; t_k \right) \right]^2. \tag{13}$$

For the identification of Θ_e and Θ_{Arr} , the corresponding data fitting problem is shown in (14). However, these two problems are non-trivial to solve, because no closed-form expression exists for U_s since the appreciably changing temperature makes sub-circuit A become a time-varying system. Instead, we resort to the built-in optimizer tool in GT-SUITE, which is a multi-

physics simulation tool to be used in our model validation in Section 4. The optimizer leverages an iterative procedure to search for global minima. Briefly speaking, it runs the model using initial guesses of the parameters. Then, it evaluates the outputs of the model against the data and determines the next estimates of the parameters. The procedure repeats itself until the achievement of convergence. What underlies the procedure is an accelerated genetic algorithm.

The above steps together constitute our parameter identification approach for the BattX model. Further remarks are as below.

Remark 1. The data fitting problems outlined in Steps 1-3 are nonlinear non-convex optimization. The non-convexity can easily get the parameter search stuck in local minima to produce physically meaningless parameter estimates. To mitigate the issue, it is sensible to constrain the search within a believably correct parameter space (Tian et al., 2020b). Specifically, one can set up approximate lower and upper bounds for every possible parameter and then limit the numerical optimization within the resultant parameter space. The prior knowledge used to establish such bounds can be derived from both experience and observation or analysis of the measurement data. Other helpful ways to overcome the local minima issue include adding regularization terms that encode prior knowledge of some parameters and applying different initial guesses to repeatedly run the numerical optimization (Tian et al., 2020b).

Remark 2. We consider a pouch cell to be used in the model validation (see Section 4) as a baseline when selecting the discharging C-rates in each step of the above approach. However, a user or practitioner may need to adjust the specific C-rates, depending on the cells to apply the model to. The overall guiding rule is yet the same—using current profiles of different C-rates to excite different dynamic processes to obtain data informative for the identification of the parameters associated with each process.

4. VALIDATION OF THE BATTX MODEL

This section shows simulation results to validate the BattX model. All simulations are carried out using GT-SUITE Version 2023, a multi-physics systems simulation platform (Gamma Technologies, LLC, 2022). GT-SUITE executes a pseudo-two-dimensional electrochemical model through the GT-AutoLion template. We set the electrochemical model to simulate an NMC811 energy-dense pouch cell with a nominal capacity of 18 Ah and run it to generate synthetic datasets. We then calibrate the BattX model using the datasets and compare its prediction performance relative to the electrochemical model.

4.1 Model Identification

The model identification procedure are as follows.

• First, the electrochemical model was run with a 0.5 C pulse load profile shown in Fig. 2. The voltage from the simulation was used to calculate R_o using (9) and then (10) to find $\hat{\Theta}_{R_o}$. The calibrated \hat{R}_o is given by

$$\hat{R}_o = -0.0383V_{s1}^3 + 0.0875V_{s,1}^2 - 0.0655V_{s,1} + 0.0226.$$

Fig. 2 compares \hat{R}_o with the benchmark truth, showing satisfactory accuracy.

 Next, the OCV-SOC relationship from the electrochemical model was transferred into the BattX table in a table

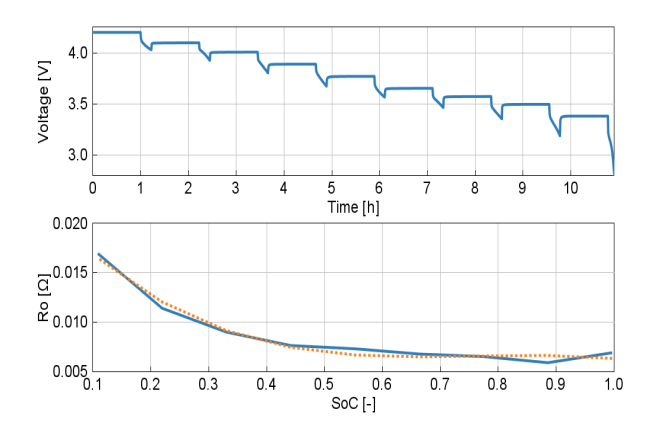


Fig. 2. Terminal voltage profile under intermittent discharging at 0.5 C to identify Θ_{R_o} and fitting of $R_o(\mathrm{SoC})$ with \tilde{R}_o based on $\hat{\Theta}_{R_o}$

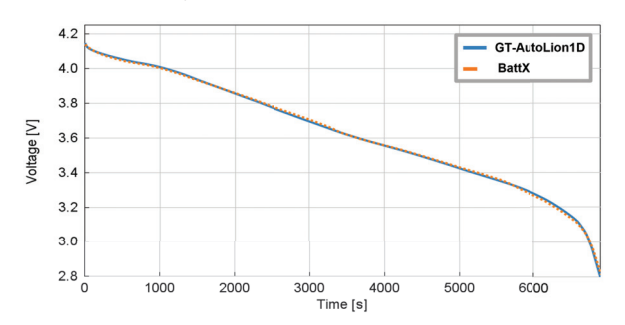


Fig. 3. Terminal voltage fitting under 0.5 C constant-current discharging based on $\hat{\Theta}_{U_s}$

lookup format. Then, using some knowledge of the electrochemical model and of the spatial discretization, we can specify

$$\lambda_i = \{1, 0.6066, 0.3115, 0.1148, 0.0164\},\$$

 $\sigma_i = \{1, 1.77, 4.00, 15.98\}.$

Then, a $0.5~\mathrm{C}$ constant-current discharge was applied to the electrochemical model. The voltage output from the simulation was used to identify $\hat{\Theta}_s$. The identified parameters are summarized in Table 1, and the comparison between the predicted terminal voltage and the benchmark is shown in Fig. 3.

Table 1. Estimation of Θ_s

	$C_{s,1}$	$R_{s,1}$
Initial Guess	33316	0.07
Lower Bound	30000	0.01
Upper Bound	35000	0.15
Optimal Value	33124	0.02

• Finally, the electrochemical model was simulated under 1.5 C and 2 C constant-current discharge loads separately. The voltage and average temperature data from the simulation were used to identify $\hat{\Theta}_{\mathrm{Th}}, \hat{\Theta}_{e}$, and $\hat{\Theta}_{\mathrm{Arr}}$. The

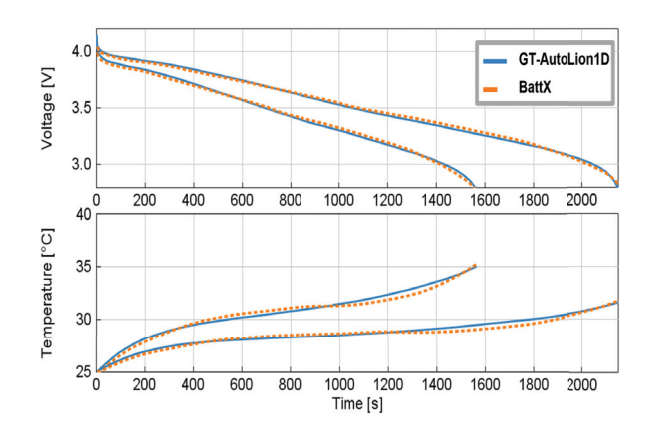


Fig. 4. Terminal voltage and temperature fitting under 1.5 C and 2 C constant-current discharging based on $\hat{\Theta}_e, \hat{\Theta}_{Th}$, and $\hat{\Theta}_{Arr}$

optimal parameters are summarized in Tables 2 and 3 with the prediction results shown in Fig. 4.

Table 2. Estimation of Θ_{Th}

	$R_{\rm surf}$	$R_{\rm core}$	C_{surf}	$C_{\rm core}$
Initial Guess	0.65	0.25	120	250
Lower Bound	0.59	0.10	100	180
Upper Bound	0.75	0.50	150	320
Optimal Value	0.71	0.12	117	189

Table 3. Estimation of Θ_e and Θ_{Arr}

	β_0	R_e	C_e	κ_1	κ_2
Initial Guess	1.2	45000	1e-4	18	40
Lower Bound	0.9	35000	8.0e-5	15.0	10.0
Upper Bound	2.0	70000	1.2e-4	22.0	50.0
Optimal Value	1.9	53088	8.6e-5	21.6	27.1

The above summarizes the identification of the BattX model. Next, we apply the identified model to new datasets to further validate it.

4.2 Model Testing and Validation

To test the predictive capability of the calibrated BattX model, we generated new datasets based on the electrochemical model. The first tests assess the model using low and high constant current discharge profiles. Fig. 5 shows the voltage prediction at $0.25~\mathrm{C}$ and $3~\mathrm{C}$ constant-current discharge. It is seen that the BattX model can deliver good accuracy in both cases.

The next dataset was generated based on a profile from the Worldwide harmonized Light vehicles Test Cycles (WLTC), which are real-world dynamometer tests by light-duty vehicles. Here, we normalized the power loads to be appropriate for the cell, supplying the cell with currents varying from -2 to 3 C. The voltage and temperature prediction by the BattX model are shown in Fig. 6, showing excellent agreement with the benchmark.

$$\hat{\Theta}_{e}, \hat{\Theta}_{Arr} = \arg\min_{\Theta_{e}, \Theta_{Arr}} \sum_{t_{k}} \left[U(t_{k}) - R_{o,T} \left(\hat{\Theta}_{R_{o}}, \Theta_{Arr}, \Theta_{Th}; t_{k} \right) I(t_{k}) - U_{s} \left(V_{s,1} \left(\hat{\Theta}_{s}, \Theta_{Arr}, \Theta_{Th}; t_{k} \right); \hat{\Theta}_{U_{s}} \right) - U_{e} \left(\Theta_{e}; t_{k} \right) \right]^{2}$$

$$(14)$$

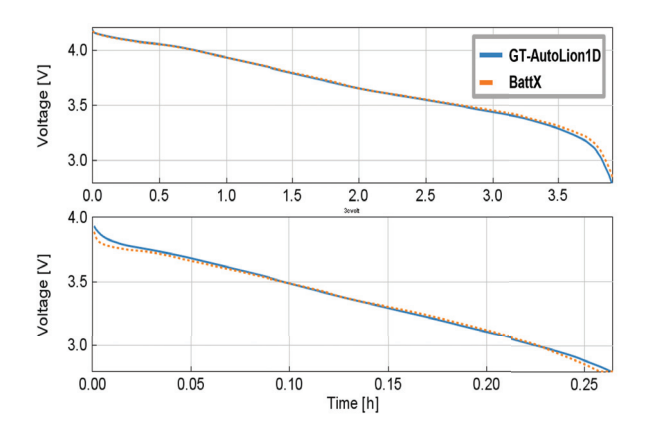


Fig. 5. Voltage prediction by the BattX model versus the benchmark truth at 0.25 C and 3 C constant-current discharge

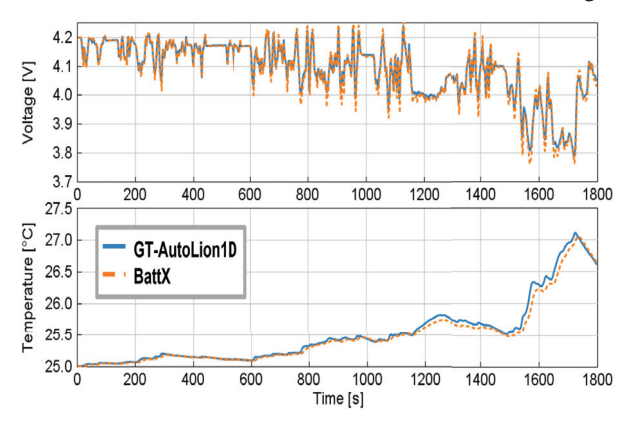


Fig. 6. Voltage and temperature prediction by the BattX model versus the benchmark results for a WLTC cycle

The third dataset was intended for LiB-powered eVTOL. Although eVTOL has attracted increasing interest as a promising solution to urban air mobility and decarbonization of aviation, conventional ECMs are hardly suitable for them, because they require high-rate discharging in the takeoff and landing phases (Bills et al., 2020). The proposed BattX model holds a promise to overcome the issue. We consider a notional eVTOL flight here, which includes three phases, takeoff, cruising, and landing. The three phases are assumed to require discharging at 2.8 C, 0.8 C, and 2.8 C. The corresponding discharging power for the considered cell is 54 W, 16 W, and 54 W, respectively. Accordingly, we generated a current load profile sequentially comprising multiple flight cycles with the three-phase pattern until the cell reaches its cutoff voltage. Fig. 7 shows that the BattX model achieves accurate prediction compared with the benchmark truth. Especially, the accuracy is found satisfactory at the times of high discharge rates. The surface temperature prediction in Fig. 7 also well agrees with the actual temperature.

To sum up, the testing and validation results show the high accuracy and fidelity of the BattX model across low to high currents in different use scenarios.

5. CONCLUSIONS

LiBs have immense impacts on contemporary society and industry. Their wide use presents a pressing demand for high-fidelity and computationally fast ECMs. This need, however, has not been met yet for applications or systems that involve

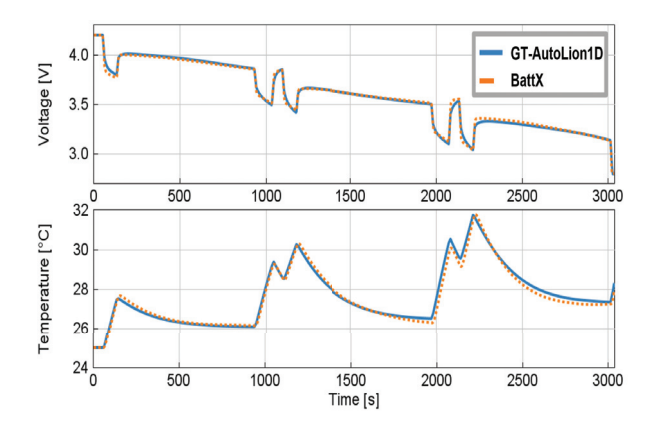


Fig. 7. Voltage and surface temperature prediction by the BattX model versus the benchmark results for multiple eVTOL cycles

charging/discharging from low to high currents. In this paper, we develop a novel ECM named BattX to fill this gap. The BattX model draws inspirations from electrochemical modeling and is characterized by using separate yet coupled circuits to simulate the electrode-phase, electrolyte-phase, and thermal dynamic processes as well as their effects on the terminal voltage. The grasp of the different key dynamics endows the model with the predictive capability to fulfill the above need. Further, a multi-pronged identification approach is custom-built for the BattX model. Extensive simulations based on different current profiles show that the model can provide accurate prediction over broad C-rate ranges. The BattX model, for the first time, expands the reach of ECMs to use scenarios that low- to high-current charging/discharging and can find potential use in various applications including eVTOLs.

REFERENCES

Biju, N. and Fang, H. (2023). BattX: An equivalent circuit model for lithium-ion batteries over broad current ranges. *Applied Energy*, 339, 120905.

Bills, A., Sripad, S., Fredericks, W.L., Guttenberg, M., Charles, D., Frank, E., and Viswanathan, V. (2020). Universal battery performance and degradation model for electric aircraft. arXiv preprint arXiv:2008.01527.

Chen, M. and Rincon-Mora, G. (2006). Accurate electrical battery model capable of predicting runtime and I-V performance. *IEEE Transactions on Energy Conversion*, 21(2), 504–511.

Doyle, M., Fuller, T.F., and Newman, J. (1993). Modeling of galvanostatic charge and discharge of the lithium/polymer/insertion cell. *Journal of The Electrochemical Society*, 140(6), 1526–1533.

Gamma Technologies, LLC (2022). *GT-SUITE User Manual*. Gamma Technologies, Westmont, IL, USA, 2022.

He, H., Xiong, R., and Fan, J. (2011). Evaluation of Lithiumion battery equivalent circuit models for state of charge estimation by an experimental approach. *Energies*, 4, 582–598.

Hu, X., Li, S., and Peng, H. (2012). A comparative study of equivalent circuit models for Li-ion batteries. *Journal of Power Sources*, 198, 359–367.

Lee, K.T., Dai, M.J., and Chuang, C.C. (2018). Temperature-compensated model for lithium-ion polymer batteries with extended Kalman filter state-of-charge estimation for an im-

- plantable charger. *IEEE Transactions on Industrial Electronics*, 65(1), 589–596.
- Li, A.G., Mayilvahanan, K., West, A.C., and Preindl, M. (2021). Discrete-time modeling of li-ion batteries with electrochemical overpotentials including diffusion. *Journal of Power Sources*, 500, 229991.
- Lin, X., Perez, H., Mohan, S., Siegel, J., Stefanopoulou, A., Ding, Y., and Castanier, M. (2014). A lumped-parameter electro-thermal model for cylindrical batteries. *Journal of Power Sources*, 257, 1–11.
- Mousavi G., S. and Nikdel, M. (2014). Various battery models for various simulation studies and applications. *Renewable and Sustainable Energy Reviews*, 32, 477–485.
- Movahedi, H., Tian, N., Fang, H., and Rajamani, R. (2022). Hysteresis compensation and nonlinear observer design for state-of-charge estimation using a nonlinear doublecapacitor li-ion battery model. *IEEE/ASME Transactions on Mechatronics*, 27(1), 594–604.
- Plett, G.L. (2015). Battery Management Systems, Volume 1: Battery Modeling. Artech House.

- Tian, N., Fang, H., and Chen, J. (2018). A new nonlinear double-capacitor model for rechargeable batteries. In Proceedings of the 44th Annual Conference of the IEEE Industrial Electronics Society, 1613–1618.
- Tian, N., Fang, H., Chen, J., and Wang, Y. (2020a). Nonlinear double-capacitor model for rechargeable batteries: Modeling, identification, and validation. *IEEE Transactions on Control Systems Technology*, 29(1), 370–384.
- Tian, N., Wang, Y., Chen, J., and Fang, H. (2020b). One-shot parameter identification of the thevenin's model for batteries: Methods and validation. *Journal of Energy Storage*, 29, 101282.
- Wang, Y., Fang, H., Zhou, L., and Wada, T. (2017). Revisiting the state-of-charge estimation for lithium-ion batteries: A methodical investigation of the extended Kalman filter approach. *IEEE Control Systems Magazine*, 37(4), 73–96.
- Weng, C., Sun, J., and Peng, H. (2014). A unified open-circuit-voltage model of lithium-ion batteries for state-of-charge estimation and state-of-health monitoring. *Journal of Power Sources*, 258, 228–237.